Journal of Cluster Science (2022) 33:985–997
https://doi.org/10.1007/s10876-021-02028-1

ORIGINAL PAPER

Facile Electro-Assisted Green Synthesis of Size-Tunable Silver Nanoparticles and Its Photodegradation Activity

N. S. Kamarudin[1] · R. Jusoh[1] · N. F. Sukor[1] · A. A. Jalil[2,3] · H. D. Setiabudi[1] · N. F. M. Salleh[4]

Received: 17 November 2020 / Accepted: 11 February 2021 / Published online: 4 March 2021
© The Author(s), under exclusive licence to Springer Science+Business Media, LLC part of Springer Nature 2021

Abstract

An eco-benign procedure was developed to synthesize ultrafine and discrete spherical shape silver nanoparticles (5–20 nm) in the presence of ionic liquid. Different types of leaves extract, including *Cymbopogon nardus*, *Polygonum minus*, *Allium Cepa*, and *Petroselinum crispum,* were used as a green reducing and capping agents for the synthesis process. The Ag nanoparticles were denoted as Ag_{CN}, Ag_{PM}, $Ag_{AC,}$ and Ag_{PC}, respectively. Notably, it was demonstrated that the Ag nanoparticles' size could simply be altered by varying the amount of total phenolic content (TPC) using different leaves. It was indicated from the characterization results that the Ag_{PC} nanoparticles' size was nine-fold smaller compared to the conventional Ag nanoparticles due to the high amount of total phenolic compounds (TPC) in the *Petroselinum crispum*. The results also revealed that ionic liquid and phenolic compounds had a synergistic effect on reducing silver ions (Ag^{+}) into silver nanoparticles (Ag) and the stabilization of the nanoparticles. The order obtained for the degradation of methylene blue (MB) was $Ag_{PC} > Ag_{PM} > Ag_{CN} > Ag_{AC} > Ag$ was influenced by a large amount of TPC and led to a decrease in particle size and enhanced photocatalytic activity. The Ag_{PC} remained effective and stable even after five subsequent cycles.

Keywords Nanoparticles · Electrochemical · Leaves extract · Photocatalytic degradation · Methylene Blue

Introduction

Photocatalytic degradation is a highly promising strategy for efficient toxic removal from contaminated water. Recently, metal nanoparticles were reported to possess the unique photocatalytic property for the degradation of organic compounds under ambient temperature with visible light illumination [1]. Metallic silver (Ag) nanoparticles are one of the ideal candidates as the photocatalyst for photocatalytic degradation due to its remarkable optical, electrical, thermal, and electromagnetic properties [2]. Numerous routes of synthesising Ag nanoparticles are present, such as gamma irradiation, chemical reduction, heat-induced reduction, reducing agents, photoreduction, microwave processing, and electrochemical method [3].

The electrolysis route has been demonstrated by Singaravelan and Bangaru Sudarsan Alwar, [4] to be a superior method for the synthesis of nanoparticles due to its high effectiveness, lower maintenance cost, and rapid achievement of the results. Nevertheless, this method usually incorporates toxic chemicals, such as ethanol, potassium nitrate (KNO_3), and poly (N-vinylpyrrolidone) in electrochemical cells, leading to environmental pollution and health risk. Hence, there is an increasing interest in substituting these organic solvents for other green solvents, which utilize bio-resources, including plants and microorganisms, for example, using the leaf extracts as a medium

Supplementary Information The online version of this article (https://doi.org/10.1007/s10876-021-02028-1) contains supplementary material, which is available to authorized users.

✉ R. Jusoh
rohayu@ump.edu.my

[1] Faculty of Chemical and Process Engineering Technology, College of Engineering Technology, Universiti Malaysia Pahang, 26300 Gambang Kuantan, Pahang, Malaysia

[2] Department of Chemical Engineering, Faculty of Chemical and Energy Engineering, Universiti Teknologi Malaysia, UTM, 81310 Johor Bahru, Johor, Malaysia

[3] Centre of Hydrogen Energy, Institute of Future Energy, UTM, 81310 Johor Bahru, Johor, Malaysia

[4] Environmental and Occupational Health Programme, School of Health Sciences, Health Campus, Universiti Sains Malaysia, 16150 Kubang Kerian, Kelantan, Malaysia

for the preparation of metal nanoparticles, such as silver, gold, platinum, and palladium [5]. Moreover, leaf extracts consist of several phenolic compounds, such as flavonoids, tannins, and gallic acid. These compounds are essential for the reduction of metal ions to metal nanoparticles [5]. Besides, phenolic compounds could also act as a capping agent that can contribute to nanoparticles' size and morphology. The presence of phenolic compounds during the synthesis process was also reported to effectively reduce the particle size, leading to an enhanced photocatalytic activity [6].

Various extraction approaches have been implemented to maximize the extraction efficiency of phenolic compounds in leaves. The most common method used is extraction, where water was used as a solvent. Nevertheless, due to the low yield production of phenolic compounds, ionic liquids (IL) were used as the alternative solvents to extract these phenolic compounds [7]. Notably, IL was recognized as a 'greener solvent,' where it possesses various attractive physicochemical properties, including low volatility, a wide temperature range in the liquid state, good dissolving ability, high thermal stability, and high ionic conductivity [8]. Furthermore, in recent years, IL also emerged as versatile and eco-friendly media for synthesizing nanoparticles due to their abundance of ions, facilitating the electrolytes for the electrolysis process [9]. Several studies reported IL has been used as both capping and reducing agents for silver nanoparticles [10, 11]. However, there has been no study which emphasizes the effects of both phenolic compound and an ionic liquid as the media for the electrosynthesis of nanoparticles. Additionally, there is no information on the mechanistic route for the synthesis of Ag nanoparticles, facilitated by phenolic compounds from leaves extract and ionic liquid.

In this study, the preparation of Ag nanoparticles (Ag_{CM}, Ag_{PM}, $Ag_{AC,}$ and Ag_{PC}) was described via the electrolysis method. In this method, IL and different types of leaves, namely *Cymbopogon nardus* (lemongrass), *Polygonum minus* (kesum), *Allium Cepa* (onions), and *Petroselinum crispum* (parsley), was used as the media during the electrolysis process. The effects of initial concentration, catalyst dosage, pH, and light on Ag nanoparticles synthesis were investigated through photocatalytic degradation. The Ag nanoparticles were characterized through X-ray powder diffraction (XRD), transmission electron microscopy (TEM), brunauer–emmett–teller (BET), and fourier transform infrared spectroscopy (FTIR).

Experimental

Material/Chemicals

Cymbopogon nardus, Petroselinum crispum, Polygonum minus, and *Allium Cepa* were obtained from Jabatan Pertanian Kuantan, Pahang. Methylene Blue and ionic liquid (IL), namely 1-Butyl-3-methylimidazolium bis(trifluoromethylsulfonyl) imide, [BMIM] [TF_2N] were purchased from Merck Sdn. Bhd. Deionized water was used as an aqueous solution. Other chemicals, including sodium oxalate (SO), isopropanol (IP), and potassium dichromate (PD), were purchased from Nano Life Quest Sdn Bhd and were used as scavenging agents. The electrode plates, Ag and Pt were obtained from Nilaco, Japan.

Preparation of Leaves Extract

All the leaves were cleaned thoroughly using distilled water, dried at 25 °C for three days, and ground into powder size of 0.25 mm-0.30 mm. 0.1 M [BMIM] [Tf_2N] solution was prepared in a 100 mL beaker. Then, 1.5 g of ground leaves were immersed in the IL solution and heated for 2 h at 60 °C. The ground leaves were then separated from the extract solution through a filtration process. Following that, this extract solution was used as a medium in the electrolysis process.

Preparation of Ag Nanoparticles

The metallic Ag nanoparticles were prepared through an electrolysis method. Two plates of an electrode, namely Ag (anode) and platinum (cathode), were used in a process where the dimension for both plates was 2 × 2 cm [12]. These plates were immersed in the extract solution where the constant current and temperature for the electrolysis process amounted to 480×10^{-3} A and 273.15 K (0 °C), respectively [12–14]. A mixed solution of leaves extract and nanoparticles was obtained from the electrolysis process. Then, the beaker stored this solution was immersed in the water bath at 80 °C before dry overnight in an oven at 110 °C. The Ag nanoparticles, which were prepared using *Cymbopogon nardus, Polygonum minus, Allium Cepa,* and *Petroselinum crispum* leaves extract, were denoted as Ag_{CN}, Ag_{PM}, Ag_{AC}, and Ag_{PC}, respectively. Meanwhile, Ag nanoparticles prepared in IL with the absence of leaves extract were denoted as Ag.

Determining the Total Phenolic Ccontents

The total amount of phenolics in the extract was determined using Folin–Ciocalteu reagent with gallic acid,

which was used as a reference standard for plotting the calibration curve. Briefly, 0.5 mL of extract solution was mixed with 2.5 mL of Folin–Ciocalteu reagent (10%). After 5 min, 2 mL of Na_2CO_3 (0.75%) was added. The mixture was then reacted for 2 h at room temperature. The absorbance was measured at 765 nm using UV–visible spectrophotometer, followed by determining the total phenolic content per gallic acid equivalent (GAE) mg sample [15].

Characterization

The absorbance of Ag nanoparticles was recorded at room temperature using Perkin Elemer U-1800 UV–Vis Spectrophotometer. Fourier transforms infrared (FTIR) spectra (Perkin Elmer Spectrum GX FTIR Spectrometer) involved a KBr method with a scan range of 500–4000 cm^{-1}. These techniques were used to identify the functional group of Ag nanoparticles. X-ray powder diffraction (XRD) ranged from 3° to 145° in 2θ scanning range with CuKα radiation and filtered by a Ni filter. This technique was used to identify the phase and crystallinity of the Ag nanoparticles. Meanwhile, the morphology and size of Ag nanoparticles were examined through the transmission electron microscopy (TEM) (JEOL JEM-2100F), and the specific surface area of the Ag nanoparticles values was calculated from the Brunauer–Emmett–Teller (BET) analysis.

Photodegradation of Methylene Blue (MB)

An investigation was conducted on the nanoparticles' photocatalytic activity in removing methylene blue (MB). These photocatalytic experiments were conducted in a Pyrex batch photoreactor consisting of 140 mm length, 85 mm diameter, and a total of 0.25 m^3. The photoreactor was also fixed with a fluorescent lamp and cooling system. Furthermore, the photocatalytic reactor set-up can be seen in Fig. S1. 200 mL of an aqueous solution of the MB dye (10 to 50 ppm), with various pH levels (3, 5, 7, 9, and 11) and amount of photocatalyst (0.002 to 0.01 g/L) was added into the reactor. Firstly, the solution was stirred in a dark surrounding for 30 min to achieve adsorption/desorption equilibrium. The solution was then exposed to visible light for 3 h. 4 mL of the solution was extracted every 30 min and centrifuged at 13,000 rpm for 10 min. After that, the UV–visible spectrophotometer was used to determine the solution's absorbance at a wavelength of 640 nm.

Results and Discussion

Total Phenolic Content (TPC)

Total phenolic content (TPC) in different leaves extract was studied, as shown in Table 1. Upon observation in this study, the amount of TPC was recorded in the order of *Petroselinum Crispum* (14,869.4 mg/kg) > *Polygonum Minus* (8296.44 mg/kg) > *Cymbopogon Nardus* (6927.56 mg/kg) > *Allium Cepa* (6145.33 mg/kg). Notably, it was found that different types of leaves had different TPC levels, which possibly influenced the synthesis process and particle size. During the synthesis process, the phenolic compounds in the extract were capable of reducing silver ions (Ag^+) to silver nanoparticles (Ag) [16]. Besides, the outstanding amount of TPC could also affect the efficiency of the MB degradation. These phenolic compounds were reported to function as a capping agent and encapsulate the Ag nanoparticles, leading to small particle size [17]. Therefore, it could be predicted that the highest amount of TPC could be exploited to achieve highly efficient MB treatment in the textile industry.

Characterization of Ag Nanoparticles

X-ray Diffraction Analysis (XRD)

The XRD patterns of Ag_{PC}, Ag_{PM}, Ag_{CN}, Ag_{AC}, and Ag are shown in Fig. 1. Several peaks were observed at 2θ values of 37.98°, 43.54°, 65.11°, and 78.15°. These values were related to (111), (200), (220), and (311) crystal planes, respectively. The peaks were positively matched with the typical peak of metallic silver based on the standard JCPDS file No. 04–0783. The appearance of sharp peaks in the XRD pattern indicated high crystallinity of silver nanoparticles (Ag). Accordingly, the involvement of phenolic compounds and IL in reducing silver ion (Ag^+) to silver nanoparticles (Ag) was perceived. The average sizes of the particles in each sample were calculated using Scherrer's formula, which is as follows:

$$D = \frac{k\lambda}{\beta \cos\theta} \quad (1)$$

Table 1 Total phenolic content of leaves extract

Leaves extract	TPC (mg/kg)*
Petroselinum crispum	14,869.4
Polygonum minus	8296.44
Cymbopogon nardus	6927.56
Allium cepa	6145.33

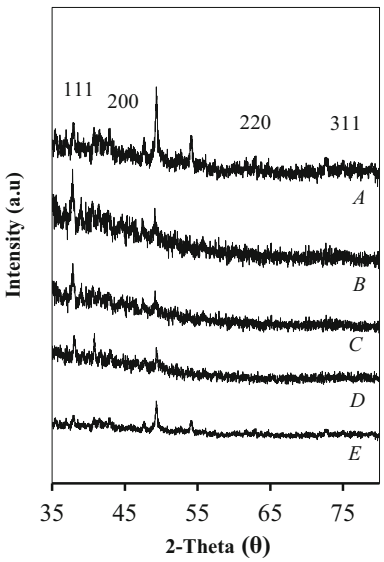

Fig. 1 XRD pattern of (A) Ag_{PC}; (B) Ag_{PM}; (C) Ag_{CN}; (D) Ag_{AC}; (E) Ag

Based on the formula above, D represents the particle's size, λ refers to the X-ray wavelength. In contrast, k refers to a dimensionless shape factor with a typical value of 0.9. Meanwhile, β represents the full width at half the maximum (FWHM) in radians of the X-ray diffraction peak, and θ refers to the Bragg angle. The average particle sizes obtained were 5.6, 8.38, 8.37, 21, and 42.02 nm, which corresponded to Ag_{PC}, Ag_{PM}, Ag_{CN}, Ag_{AC}, and Ag. Based on the observation, the particle size was influenced by the type of leaves extract used for the synthesis process.

Nevertheless, the size of particles (6–20 nm) was smaller when leaf extracts were used to synthesize nanoparticle compared with the synthesized nanoparticles in IL with the absence of leaf extracts, which was 42 nm. These results suggested that even IL can be used as a capping agent. With the absence of the leaf extract, the size of nanoparticles produced was relatively larger than the size of nanoparticles produced under the presence of leaves extract. Ultimately, leaf extract with high phenolic compounds along the IL can significantly promote smaller nanoparticle sizes.

Transmission Electron Microscopy (TEM)

Figure 2a–d illustrates the TEM image of Ag_{PC}, Ag_{PM}, Ag_{CN}, and Ag_{AC}, each with an average size of 6 nm, 8 nm, 9 nm, and 24 nm, respectively. It was also seen from the TEM image that most of the Ag nanoparticles were discrete and well dispersed. However, the TEM image in Fig. 2e indicates that Ag nanoparticles were agglomerated, leading to a larger nanoparticle size of 51 nm. This observation proves that leaves extract's phenolic compounds possessed an outstanding tenacity against aggregation [16, 18]. Similar results were also obtained from the XRD analysis. To be specific, Ag_{PC} was identified with the smallest nanoparticle size, while the Ag sample, which was synthesized without leaf extract, was identified with a larger nanoparticle size. In addition, the calculated value of particle–particle distance (d_{pp}) was obtained in the order of $Ag_{PC} > Ag_{PM} > Ag_{CN} > Ag_{Ac} > Ag$. This order indicated that the smallest nanoparticle size possesses the highest d_{pp} values. As previously mentioned, the small size of nanoparticles may be due to the phenolic compounds' ability to encapsulate the surface particle and develop a discrete particle [19–21]. Therefore, it was proven that phenolic compounds in the leaves extract could significantly influence the catalyst's size and structure.

BET Surface Area Analysis

The surface areas of the Ag nanoparticle were analyzed to determine the catalytic activity of nanoparticles. Based on the BET analysis in Table 2, the specific surface areas were calculated as 8.14 m^2/g, 9.34 m^2/g, 17.22 m^2/g, 33.32 m^2/g, and 37.10 m^2/g for Ag, Ag_{AC}, Ag_{CN}, Ag_{PM}, and Ag_{PC}, respectively. It was shown from the TEM analysis that Ag_{PC} had the smallest particle size, while Ag had a larger particle size. It was shown from these results that small particles resulted in a larger surface area of the catalyst. A previous argument could support this finding that phenolic compounds contributed to a larger surface area of the catalyst [20].

It was proven in the results in Fig. 3 that the amount of TPC influenced nanoparticle size in the leaves extract. Remarkably, it can be significantly observed that the average size of Ag_{PC}, Ag_{PM}, Ag_{CN}, and Ag_{AC} was nine-fold, six-fold, five-fold and two-fold smaller than the size of Ag nanoparticle, respectively. The difference in size was due to the different amount of phenolic content were present in *Petroselinum crispum, Polygonum minus, Cymbopogon nardus,* and *Allium Cepa* extract which were used to encapsulate the Ag_{PC}, Ag_{PM}, Ag_{CN}, and Ag_{AC} nanoparticle. Subsequently, a small nanoparticle size was obtained, which later increased the nanoparticle's surface area. Therefore, it can be concluded that different amounts of phenolic content from other types of leaves significantly influence the size of nanoparticles.

Fourier Transform Infrared (FT-IR)

Figure 4 demonstrated FTIR spectroscopy measurements, which were conducted to identify the functional group present in the synthesized Ag nanoparticle and the possible pathway of biosynthesis of Ag nanoparticle. A peak at 3315 cm^{-1} was shown from the FTIR spectra of

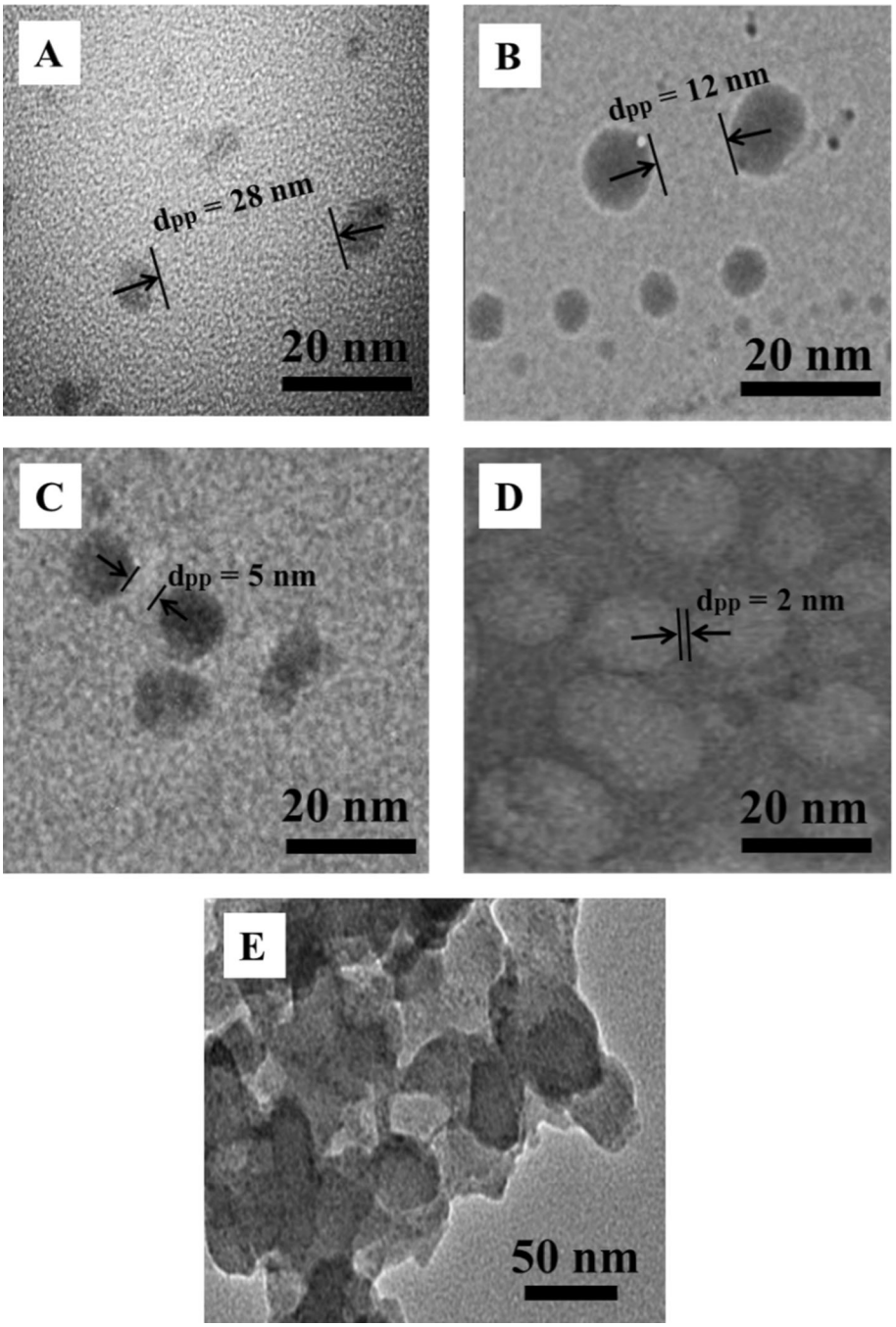

Fig. 2 TEM image of **a** Ag_{PC}; **b** Ag_{PM}; **c** Ag_{CN}; **d** Ag_{AC}; **e** Ag

Table 2 Textural properties of catalysts

Catalyst	Surface area (m^2/g)	Size (nm)
Ag_{PC}	37.10	5.60
Ag_{PM}	33.32	8.37
Ag_{CN}	17.22	8.38
Ag_{AC}	9.34	21.01
Ag	8.14	42.02

Polygonum minus, Cymbopogon nardus, Allium Cepa, and *Petroselinum crispum* leave extracts, indicating the presence of O–H stretching of polyphenol. These leaf extracts were considered as active reducing agents for nanoparticle synthesis [22]. Meanwhile, a sharp peak at 1636 cm^{-1} and a trivial peak at 1150 cm^{-1} were obtained due to the stretching of the carboxyl (–C=O) group and (–C–O) ether linkage [23, 24].

FTIR band at 3580 (–OH), 2967 (C–H), 1465 (C=C), 1178 (C–O), and 509 (M–O) represented the synthesized

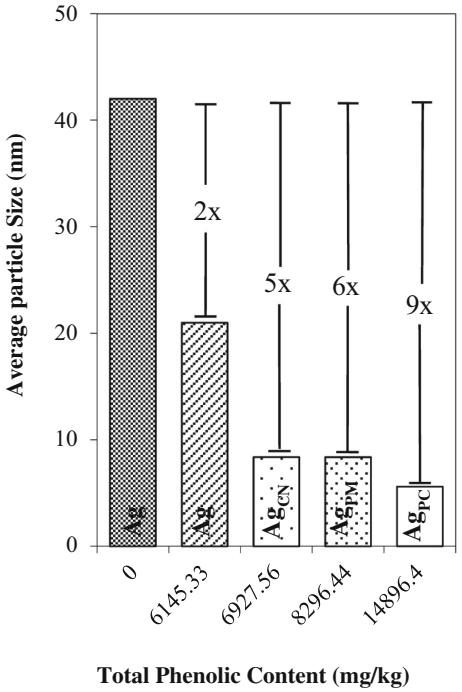

Fig. 3 Total phenolic content vs average particle size of Ag nanoparticle

Ag nanoparticle before drying. Meanwhile, the band at 3630 (–OH), 1683 (C=O), 1475 (C=C), 1188 (C–O), and 511 (M–O) represented the Ag, which was synthesized after drying in the oven at 110 °C temperature level. It was found that the presence of hydroxyl stretching vibration for Ag was synthesized by the leaves extract, indicating the presence of –OH functional groups in phenolic compounds [25]. Furthermore, it was proven that peak intensity was reduced and became broader when Ag nanoparticle was dried since the dried nanoparticle often physically absorbs water [26]. Then, the peak which appeared at 1465 cm^{-1} and 1475 cm^{-1} were assigned to C=C stretch in the aromatic ring [27], while the small peak at 2967 cm^{-1} occurred due to the C–H stretching vibrations of the imidazolium ring in ionic liquid. Moreover, the intense peak around 1178 cm^{-1} and 1188 cm^{-1} was due to the C–O ether linkage formed by reducing Ag^{+} to Ag by *Polygonum minus, Cymbopogon nardus, Allium Cepa*, and *Petroselinum crispum* leaves extract. Additionally, the carbonyl group of C=O stretching vibration was also present at the absorption peak of 1683 cm^{-1}. Upon reduction, a new peak was observed at 511 cm^{-1} (M–O).

Based on the FTIR spectral analysis of Ag nanoparticle, the possible mechanism of green synthesis of Ag nanoparticle through leaf extract in the presence of IL is presented in Fig. 5. Several phytochemicals, namely phenols, protein, tannin, gallic acid, and flavonoids, are demonstrated in a single plant cell, including *Polygonum minus, Cymbopogon nardus, Allium Cepa*, and *Petroselinum crispum* [28]. It was suggested in a previous

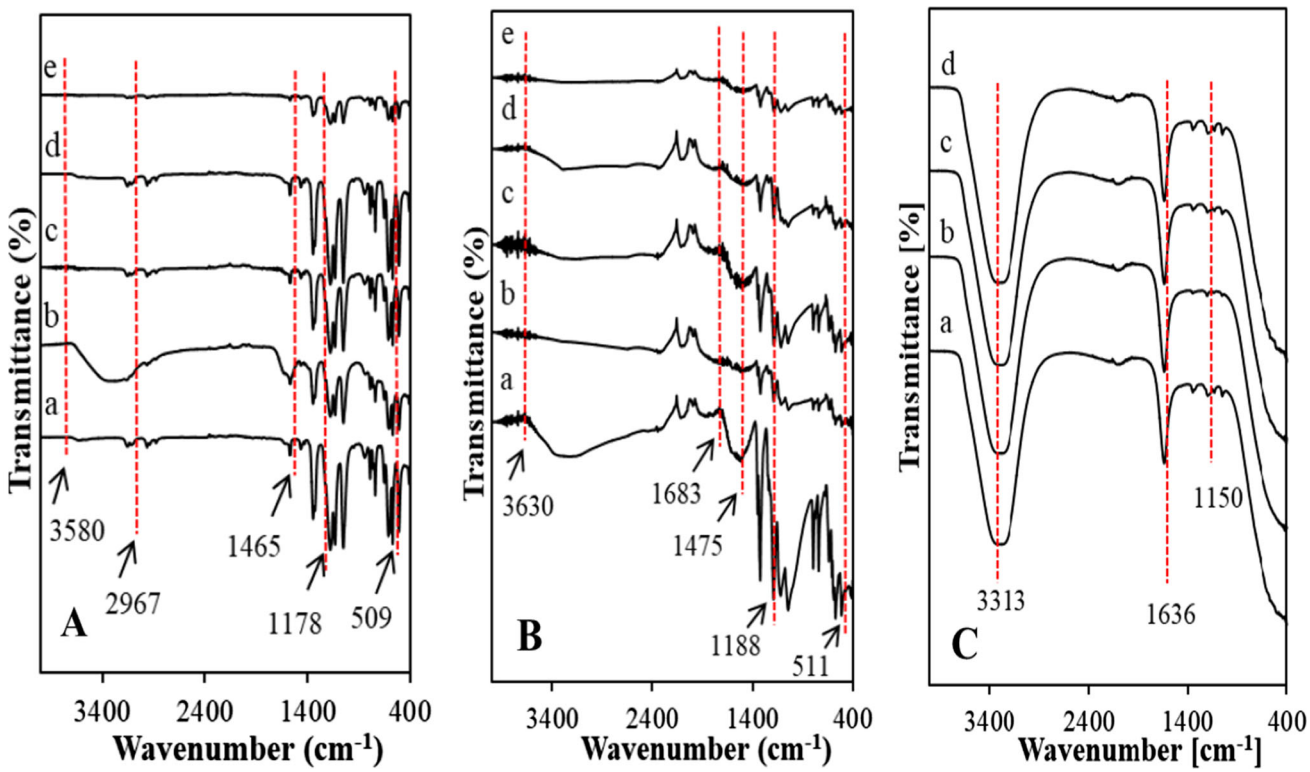

Fig. 4 FT-IR spectra of (a) Ag; (b) Ag_{PM}; (c) Ag_{CN}; (d) Ag_{AC}; (e) Ag_{PC} leaf extract **A** Before Drying, **B** After Drying; and **C** Leaves Extract

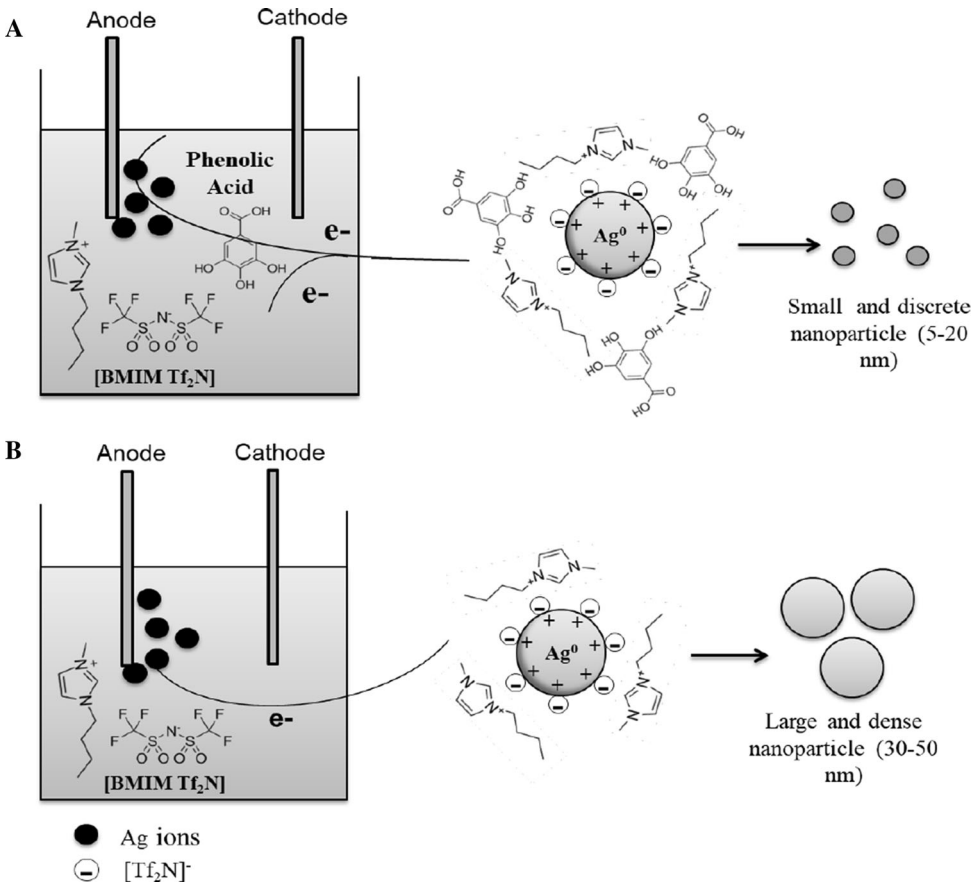

Fig. 5 Possible mechanism of electro–synthesis of Ag nanoparticle **a** in leaves extract and **b** without leaves extract

study that phenolic compounds were possibly the factors of the reduction and subsequent stabilization of silver ions [29, 30]. Phenolic compounds also possess antioxidant properties capable of donating electron and hydrogen atoms [31, 32]. Furthermore, free radicals at the radical center of both the electron–donor and electron-withdrawing groups were highlighted.

Additionally, the stability of free radicals is enhanced. This phenomenon is known as the *captodative* effect. In phenolic compounds, the electron-donating OH group's presence in the *ortho*–position and the electron-withdrawing –COOH group in the *para*–position stabilizes the radical with a large number of resonance forms. As shown in Fig. 5a, silver ion was reduced by hydroxyl groups of phenolic compounds during the reduction reaction. The reduction process was also proven from the FTIR analysis as the –OH group peak shifted from 3313 to 3580 cm^{-1}. This shift was due to the presence of enol in the phenolic compounds, which formed an intermediate silver complex with silver ion before its oxidization into a quinonoid form. Notably, the OH bands in quinonoid were known for their significant strength and higher polarisation [33].

As discussed in XRD and TEM analysis, the presence of phenolic compounds in the reaction mixture did not only reduce Ag ions; it also possessed a capping ability, leading to the formation of small-sized Ag nanoparticle. Moreover, the surface capping of nanoparticle was not only accomplished by the phenolic compounds present in leaves extracts, but the IL in the solution also facilitated the stability and formation of diminutive nanoparticle [34]. The interactions between Ag and the ionic anion were previously investigated by Corrêa et al. [11]. It was found that the free-anion state of IL was due to the formation and stabilization of the Ag nanoparticles. This possible interaction was due to the partial positive charge of the surface Ag nanoparticles through $[Tf_2N]^-$ free ions [35]. Also, IL could disrupt the immediate contact of particles of two substrates. Therefore, they could function as agglomeration inhibitors. Based on the synthesis of Ag nanoparticle, it was proposed that both IL and phenolic compounds in the leaves extract encapsulated the surface of the Ag catalyst. With these compounds, the Ag catalyst was set apart to prevent aggregation and control particles' growth for a stable silver colloidal suspension [31]. However, in Fig. 5b, it could be observed that a larger nanoparticle size was obtained due to the absence of phenolic compound-based synthesis media from the reaction process. In this condition, only IL was present as the capping agents, which were not adequate to encapsulate and control nanoparticle growth. This condition explained the condition where Ag's

synthesis using leaf extract led to smaller nanoparticle size than the Ag synthesized without the leaves extract.

Photocatalytic Testing on the Degradation of Methylene Blue (MB)

Performance of Catalyst Using Different Types of Leaves

The Ag nanoparticles' performance was examined through the decolorization of MB, as shown in Fig. 6. It could be seen that Ag_{PC} exhibited the highest degradation of MB at 65.61%, followed by Ag_{PM} at 60.98%, Ag_{CN} at 34.86%, Ag_{AC} at 28.50%, and Ag at 14.92%. Specifically, Ag_{PC} displayed an outstanding photocatalytic performance as it possessed the highest amount of TPC compared to other catalysts. The higher content of phenolics in leaf extract, the better the photocatalytic activity of silver nanoparticles. The highest amount of phenolic in Ag_{PC} was predicted to function as capping agents to suppress the size of particles and subsequently increase the surface area. It was perceived that the surface area of the Ag catalyst became the continuation of the photocatalytic activity of methylene blue, as proven in the BET analysis. The expansion in the surface area led to an increase in the nanoparticles' absorption capacity [34]. As the surface area per mass of the material increased, a higher amount of the material could contact the surrounding materials, leading to enhanced photocatalytic activity. Meanwhile, the Ag nanoparticle synthesized without leaf extract exhibited a smaller surface area. As a result, the photocatalytic activity was disrupted. The results further supported the previous argument that the total phenolic compound in the leaves extracts indeed influenced the efficiency of the MB degradation.

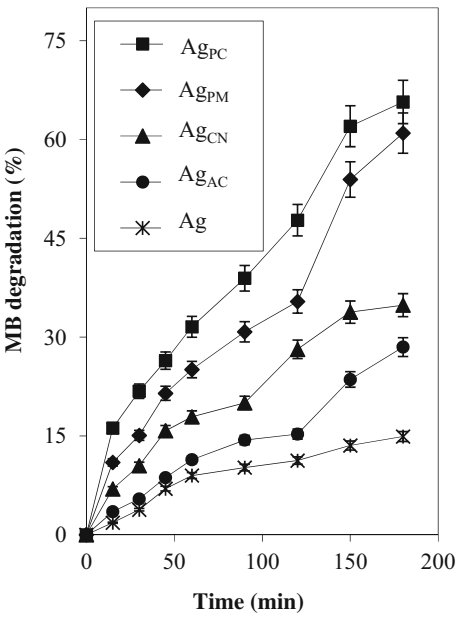

Fig. 6 Performance of catalyst using different types of leaves (Conc = 20 ppm, pH = 5, Light = Visible, Ag = 0.01 g/L)

Effect of pH and Catalyst Dosage

The pH of a solution plays a vital role in the photocatalytic process of various pollutants. The effect of pH on methylene blue photodegradation was studied at a range of pH values from 3 to 12. In this investigation, the Ag nanoparticles (0.01 g L^{-1}) with a dye concentration of 20 mg L^{-1} was used. Based on the result in Fig. S2(A), the highest percentage of removal methylene blue was found at pH 9. It was indicated from the graph pattern that the increase in pH led to the improvement in the photocatalytic activity. However, the degradation efficiency started to decrease at some point in the pH increase. This decrease was due to the electrostatic interaction between the nanoparticle's surface charge and the charge on the dye molecule [36], which was based on a zero-point charge (pH_{pzc}). As the pH_{pzc} was found to amount to pH 6.3 [37], the Ag nanoparticle surface would be positively charged in acidic media at lower pH values (pH < 6.3). However, the Ag nanoparticle surface was negatively charged under alkaline conditions (pH > 6.3). As MB was a cationic dye, a high pH level facilitated the absorption of dye molecule on the nanoparticle surface, which resulted in high degradation efficiency. Therefore, higher degradation of MB was observable in alkaline conditions compared to acidic conditions.

Figure S2(B) presents the effect of catalyst dosage on the degradation of methylene blue, which was investigated within the range of 0.01 to 0.06 g/L. It was observed that the highest percentage of removal was achieved when 0.02 g/L of nanoparticle was used. Furthermore, the degradation efficiency significantly increased from 77.06% to 99.41% due to increased catalyst dose from 0.01 to 0.02 g/L. As the catalyst loading increased, the number of active sites and the number of photons and dye being absorbed also took place, which eventually enhanced the degradation efficiency [38]. However, when the catalyst dose was increased further to 0.04 g/L, the degradation efficiency was reduced to 54.1%. This reduction was due to the excessive amount of catalyst loading, leading to the blockage of sunlight and disrupting photocatalyst irradiation [39]. As a result, the hydroxyl free radicals ($OH^{\cdot}$) could not be produced, and the photocatalytic process was inhibited [40]. It was also reported in a previous study that the amount of photocatalyst exceeded the optimum dosage, resulting in a negative impact on the degradation efficiency. The summaries of the degradation of various pollutants using Ag nanoparticles as photocatalyst are presented in Table 3 [41–49].

Effect of Scavenging

The mechanism of photodegradation was investigated by conducting experimental studies on the effects of scavenging agents. In this study, the scavengers such as potassium dichromate (PD), isopropanol (IP), and sodium oxalate (SO) were used to scavenge the radicals, including photogenerated electrons, hydroxyl radicals ($^{\cdot}$OH), and photogenerated holes (h^+), respectively. Based on Fig. S3, the highest percentage of MB degradation at 99.41% was obtained from the system with the scavenging agent's absence. However, with the presence of scavengers, the efficiency of the photocatalytic activity decreased. Furthermore, the percentage of MB degradation was reduced tremendously to 19.49% and 47.42% with the incorporation of SO and IP to the reaction, respectively. This pattern proved that the photogenerated holes (h^+) and $OH^{\cdot}$ radical had an essential role in the degradation of MB. Meanwhile, by adding PD to the system, the photocatalytic efficiency only decreased to 68.44%, indicating that a high percentage of MB degradation was still achievable even after the photogenerated electrons (e^-) were scavenged. Overall, it was proven that photogenerated electrons (e^-) do not significantly affect the degradation rate of MB in the photocatalytic reaction.

The photocatalytic reaction took place upon Ag nanoparticles' irradiation, leading to the excitation of valence band (VB) electrons to the conduction band (CB). Silver nanoparticles exhibit a unique phenomenon of Surface Plasmon Resonance (SPR). Hence, many electron–hole (e^-–h^+) pairs were generated due to the SPR effect of the Ag nanoparticles [50]. The scavenging study showed that h^+ and ·OH were primarily responsible for the degradation of MB. Thus, a reaction was created between the photogenerated holes (h^+) in the valence band and with water (H_2O), leading to the production of hydroxyl radicals ($OH^{\cdot}$) as shown in Eq. (2). In this case, the hydroxyl radical ($OH^{\cdot}$) generated from the reaction functioned as a powerful oxidizer to degrade MB and convert them into CO_2 and H_2O, as illustrated in Eq. (3) [51].

$$H_2O + h^+ \rightarrow \cdot OH \quad (2)$$

$$\cdot OH + MB \rightarrow \text{degraded products} \rightarrow CO_2 + H_2O \quad (3)$$

Kinetic Studies

In this study, a series (10, 40, 60, 80 mg/L) of the MB solution was prepared with 0.02 g/L of Ag_{PM} was added into the reactor. As shown in Table 4, degradation efficiency decreased with the increase in the initial MB concentration. This phenomenon could be explained based on change in the optical density of the MB solution at various concentrations. As the initial concentrations of the dye increased, the degradation efficiency of the MB was diminished. It might be due to the absorption of a high concentration of the MB molecules on the catalyst's surface, leading to a significant amount of light being absorbed by the MB molecules compared to the Ag particles. Therefore, the penetration of light to the catalyst's surface decreased, which eventually reduced the formation of the hydroxyl radicals. These radicals had an important role in

Table 3 Summary of recently used Ag nanoparticles for degradation of various pollutants

Model organic pollutant	Reaction condition				Kinetics	Degradation Efficiency (%)	Source
	Catalyst amount	Concentration pollutant	pH	Time irradiation			
2, 4–dicholorophenoxyacetic acid	0.009 g/L	8.15 ppm	3.24	180 min	Pseudo-first-order	97.8	[41]
Methyl orange and Coomassie brilliant blue G-250	20 mg	10 ppm	–	10 h and 6 h	–	> 60 and > 70	[42]
p-nitrophenol	0.5 g/L	5 ppm	6	–	First order	98	[43]
Brilliant green dye	10 mg	15 ppm	7.9	20 min	–	80	[44]
2, 4–dicholorophenoxyacetic acid	0.01 g/L	10 ppm	3	180 min	Pseudo-first-order	99.78	[45]
Eosin-Y	50 mg	10 ppm	–	60 min	–	> 97	[46]
Bengal dye	0.25 g	20 ppm	–	2 h	–	83	[47]
Reactive blue 19 (RB19) and reactive yellow 186 (RY186)	10 mg	30 ppm	–	180 min	Pseudo-first-order	88% and 86%	[48]
Methylene blue	1 mg/mL	5 ppm	11	60 min	First-order	29.09	[49]
Methylene blue	0.02 g/L	20 ppm	9	180 min	Zero-order	99.41	This work

Table 4 Values of the squared correlation coefficient and rate constant for photocatalytic degradation of MB

Initial concentration of MB (mg L^{-1})	MB degradation (%)	First order kinetic ($\ln (C_0/C_t) = kt$)		Second order kinetic ($1/C_t - 1/C_0 = kt$)	
		k_1 (min^{-1})	R_1^2	k_2 (L mg^{-1} min^{-1})	R_2^2
10	97.37	0.0144	0.823	0.0104	0.427
40	96.00	0.0142	0.900	0.0018	0.549
60	93.29	0.0128	0.924	0.0008	0.683
80	91.92	0.0114	0.915	0.0005	0.643

the degradation of MB. The kinetic of MB degradation using Ag nanoparticles was investigated using first, and second-order kinetic reactions [52]. The general rate law expressions are given by Eq. (4):

$$-\frac{d(MB)}{dt} = k_r(MB)^n \tag{4}$$

After considering 1st order reaction (n = 1) and 2nd order reaction (n = 2), Eq. (4) was integrated and simplified to first–order and second-order equation (Eqs. 5 and 6) as reported by other studies [53, 54].

$$\ln\frac{(MB)_0}{(MB)_t} = k_1 t \tag{5}$$

$$\frac{1}{(MB)_t} - \frac{1}{(MB)_0} = k_2 t \tag{6}$$

Accordingly, MB_0 represents the initial concentration of MB and MB_t, signifying the MB concentration at t time. Meanwhile, k_1, and k_2 represent the reaction rate constant. The graphs of different MB concentrations at 10, 40, 60 and 80 ppm were plotted according to first and second-order kinetic reactions, as demonstrated in Fig. 7. The first-order rate constant (k_1), and second-order rate constants (k_2) were determined from the plots of $\ln (C_0/C_t)$ against time and $(1/C_t) - (1/C_0)$ versus time, respectively. The values of k_1 and k_2 and correlation coefficients (R^2) were calculated and summarized Table 4. As might be seen in this table, it reveals that the photocatalytic degradation of MB followed first-order kinetic ($R^2 > 0.92$), which is confirmed by satisfactorily high R^2 values. Meanwhile, the second-order kinetic ($R^2 > 0.68$) revealed lower R^2 values, which indicated the experimental data are not in agreement with the kinetic model. The obtained results also displayed that the reaction rate constant had a significant decrease in the degradation performance as the MB concentration increased. This is due to the high concentration of MB molecules on the surface of the Ag catalyst that caused shielding of light radiation [55]. As a result, the amount of generated radical on the surface of photocatalyst reduced which led to the decrease in the degradation efficiency [56].

Reusability

Five consecutive runs of the investigation were conducted on the reusability and recovery of the Ag catalysts in MB degradation. As illustrated in Fig. 8, desirable reusability was found in the catalyst, with only a minor reduction in its activity. The Ag catalyst still could be reused for five consecutive cycles after being separated from the reaction solution through filtration, several rounds of washing with deionized water and drying in the oven. As a result, an overall 17% of loss in MB degradation was found after the fifth cycle demonstrated this catalyst's stability and reusability. Besides, declining photocatalytic efficiency was due to decreased active site after the absorption of pollutants into the Ag catalyst.

Conclusion

In conclusion, silver nanoparticles (Ag) were successfully prepared via eco–benign electrochemical method in the presence of IL using different types of leaves extract as the media, namely *Cymbopogon nardus, Polygonum minus, Allium Cepa*, and *Petroselinum crispum*. It was revealed from the nanoparticle's physicochemical properties by XRD, TEM, FTIR, and BET that the introduction of ionic liquid and leaves extract during the synthesis process led to a significant reduction of silver ions (Ag^+) into silver nanoparticle (Ag). The results also demonstrated that the Ag nanoparticles were discrete and well dispersed with an average size of 6 nm, 8 nm, 9 nm, and 24 nm for Ag_{PC}, Ag_{PM}, Ag_{CN}, and Ag_{AC}. Hence, it was remarkably proved that the Ag nanoparticles' size could simply be altered by varying the amount of total phenolic content (TPC) using different leaves. The Ag_{PC} displayed the highest MB degradation at 65.61%, followed by Ag_{PM} at 60.98%, Ag_{CN} at 34.86%, Ag_{AC} at 28.50%, and Ag at 14.92%. This result was obtained because the high amount of phenolics in Ag_{PC} led to small particle size and large surface area, which significantly enhanced the photocatalytic activity of the Ag_{PC} nanoparticle. Moreover, the optimum condition

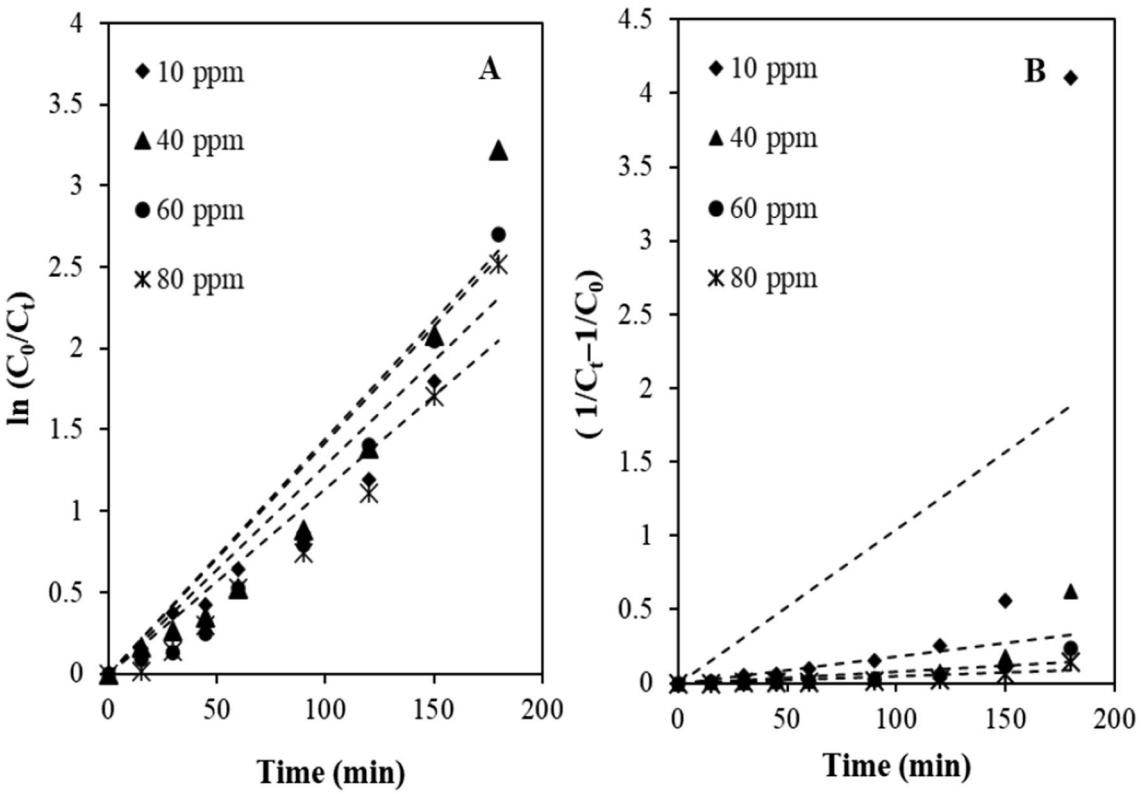

Fig. 7 The plot of **a** first order and **b** second order kinetic

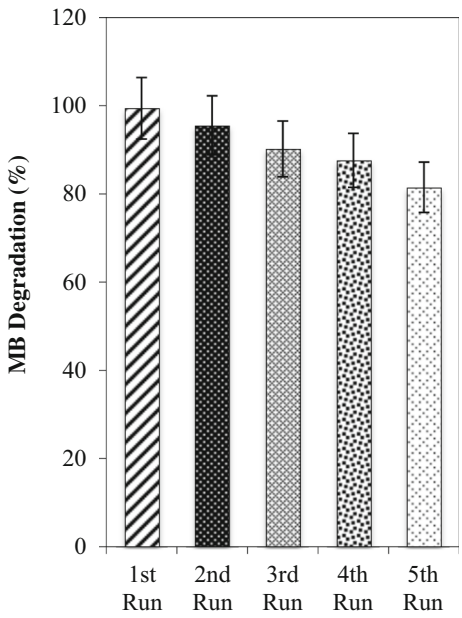

Fig. 8 Reusability of Ag nanoparticle on degradation MB degradation (MB = 20 ppm, pH 9, Ag_{PC} = 0.02 g/L)

of the Ag_{PC} nanoparticle was obtained at pH 9, 0.02 g L^{-1} of catalyst dosage, and 20 mg L^{-1} of MB initial concentration. It was demonstrated from the kinetics studies that the photodegradation of MB through Ag_{PC} nanoparticle was based on first-order kinetic reaction. Meanwhile, it was found from the scavenging study that photogenerated hole (h^+) had a crucial role in photocatalytic reaction. It was also revealed from the photocatalyst reusability that the catalyst remained stable even after five cycles. Therefore, it was implied that the silver nanoparticle (Ag) could be developed into an effective catalyst to be applied in the degradation of biological wastewater treatment.

Acknowledgements A token of appreciation goes to the financial support by University Malaysia Pahang through the Internal University Grant (Grant No. RDU1903130) and Collaboration Research Grant (Grant No. RDU182302).

References

1. G. Ganapathy Selvam and K. Sivakumar (2015). Phycosynthesis of silver nanoparticles and photocatalytic degradation of methyl orange dye using silver (Ag) nanoparticles synthesized from *Hypnea musciformis* (Wulfen) J.V. Lamouroux. *Appl. Nanosci.* **5**, 617–622. https://doi.org/10.1007/s13204-014-0356-8.
2. I. Khan, K. Saeed, and I. Khan (2019). Nanoparticles: properties, applications and toxicities. *Arab. J. Chem.* **12**, 908–931. https://doi.org/10.1016/j.arabjc.2017.05.011.
3. S. Iravani, H. Korbekandi, S. V. Mirmohammadi, and B. Zolfaghari (2014). Synthesis of silver nanoparticles: chemical, physical and biological methods. *Res. Pharm. Sci.* **9**, 385–406.
4. R. Singaravelan and S. Bangaru Sudarsan Alwar (2015). Electrochemical synthesis, characterisation and phytogenic properties

of silver nanoparticles. *Appl. Nanosci.* **5**, 983–991. https://doi.org/10.1007/s13204-014-0396-0.
5. L. M. Carrillo-López, R. M. Soto-Hernández, H. A. Zavaleta-Mancera, and A. R. Vilchis-Néstor (2016). Study of the performance of the organic extracts of *Chenopodium ambrosioides* for Ag nanoparticle synthesis. *J. Nanomater.* **2016**, 4714162. https://doi.org/10.1155/2016/4714162.
6. M. M. Khan, N. H. Saadah, M. E. Khan, M. H. Harunsani, A. L. Tan, and M. H. Cho (2019). Potentials of Costus woodsonii leaf extract in producing narrow band gap ZnO nanoparticles. *Mater. Sci. Semicond. Process.* **91**, 194–200. https://doi.org/10.1016/j.mssp.2018.11.030.
7. H. Passos and M. Freire (2014). Ionic liquid solutions as extractive solvents for value-added compounds from biomass. *Green Chem.* **46**, 4786–4815. https://doi.org/10.1039/C4GC00236A.
8. M. Smiglak, J. Pringle, X. Lu, L. Han, S. Zhang, H. Gao, D. MacFarlane, and R. Rogers (2014). Ionic liquids for energy, materials, and medicine. *Chem Commun (Camb)*. https://doi.org/10.1039/c4cc02021a.
9. G. Park, J. Park, Y. Cho, and C. Lee (2016). Palladium nanoparticles synthesized by pulsed electrolysis in room temperature ionic liquid. *Int. J. Electrochem. Sci.* **11**, 4539–4549.
10. E. Husanu, C. Chiappe, A. Bernardini, V. Cappello, and M. Gemmi (2018). Synthesis of colloidal Ag nanoparticles with citrate based ionic liquids as reducing and capping agents. *Colloids Surf. A* **538**, 506–512. https://doi.org/10.1016/j.colsurfa.2017.11.033.
11. C. M. Corrêa, M. A. Bizeto, and F. F. Camilo (2016). Direct synthesis of silver nanoparticles in ionic liquid. *J. Nanoparticle Res.* **18**, 132. https://doi.org/10.1007/s11051-016-3436-8.
12. N. Syahirah Kamarudin, R. Jusoh, H. DinaSetiabudi, and N. FatehaSukor (2018). Photodegradation of methylene blue using phyto-mediated synthesis of silver nanoparticles: effect of calcination treatment. *Mater. Today Proc.* **5**, 21981–21989. https://doi.org/10.1016/j.matpr.2018.07.059.
13. R. Jusoh, A. Abdul Jalil, S. Triwahyono, and N. H. Kamarudin (2015). Synthesis of dual type Fe species supported mesostructured silica nanoparticles: synergistical effects in photocatalytic activity. *RSC Adv*. https://doi.org/10.1039/C4RA13837F.
14. R. Jusoh, A. Abdul Jalil, S. Triwahyono, A. Idris, and N. Mohd Yusof (2015). Photodegradation of 2-chlorophenol over colloidal α-FeOOH supported mesostructured silica nanoparticles: influence of a pore expander and reaction optimization. *Sep Purif Technol*. https://doi.org/10.1016/j.seppur.2015.05.017.
15. S. Fattahi, E. Zabihi, Z. Abedian, R. Pourbagher, A. Motevalizadeh Ardekani, A. Mostafazadeh, and H. Akhavan-Niaki (2014). Total phenolic and flavonoid contents of aqueous extract of stinging Nettle and in vitro antiproliferative effect on Hela and BT-474 cell lines. *Int. J. Mol. Cell. Med.* **3**, 102–107.
16. A. Zuorro, A. Iannone, S. Natali, and R. Lavecchia (2019). Green synthesis of silver nanoparticles using bilberry and red currant waste extracts. *Processes.* **7**, 193. https://doi.org/10.3390/pr7040193.
17. S. P. Goutam, G. Saxena, V. Singh, A. K. Yadav, R. N. Bharagava, and K. B. Thapa (2018). Green synthesis of TiO_2 nanoparticles using leaf extract of *Jatropha curcas* L. for photocatalytic degradation of tannery wastewater. *Chem. Eng. J.* **336**, 386–396. https://doi.org/10.1016/j.cej.2017.12.029.
18. S. Y. Lee, S. Krishnamurthy, C.-W. Cho, and Y.-S. Yun (2016). Biosynthesis of gold nanoparticles using ocimum sanctum extracts by solvents with different polarity. *ACS Sustain. Chem. Eng.* **4**, 2651–2659. https://doi.org/10.1021/acssuschemeng.6b00161.
19. R. Jusoh, A. A. Jalil, S. Triwahyono, A. Idris, S. Haron, N. Sapawe, N. F. Jaafar, and N. W. C. Jusoh (2014). Synthesis of reverse micelle α-FeOOH nanoparticles in ionic liquid as an only electrolyte: inhibition of electron–hole pair recombination for efficient photoactivity. *Appl. Catal. A Gen.* **469**, 33–44. https://doi.org/10.1016/j.apcata.2013.09.046.
20. M. Harshiny, C. N. Iswarya, and M. Matheswaran (2015). Biogenic synthesis of iron nanoparticles using *Amaranthus dubius* leaf extract as a reducing agent. *Powder Technol.* **286**, 744–749. https://doi.org/10.1016/j.powtec.2015.09.021.
21. G. Sharmila, S. Haries, M. Farzana Fathima, S. Geetha, N. Manoj Kumar, and C. Muthukumaran (2017). Enhanced catalytic and antibacterial activities of phytosynthesized palladium nanoparticles using *Santalum album* leaf extract. *Powder Technol.* **320** (2017), 22–26. https://doi.org/10.1016/j.powtec.2017.07.026.
22. S. Firoozi, M. Jamzad, and M. Yari (2016). Biologically synthesized silver nanoparticles by aqueous extract of Satureja intermedia C.A. Mey and the evaluation of total phenolic and flavonoid contents and antioxidant activity. *J. Nanostruct. Chem.* **6**, 357–364. https://doi.org/10.1007/s40097-016-0207-0.
23. T. N. J. I. Edison, Y. R. Lee, and M. G. Sethuraman (2016). Green synthesis of silver nanoparticles using *Terminalia cuneata* and its catalytic action in reduction of direct yellow-12 dye. *Spectrochim. Acta A* **161**, 122–129. https://doi.org/10.1016/j.saa.2016.02.044.
24. T. J. I. Edison and M. G. Sethuraman (2013). Biogenic robust synthesis of silver nanoparticles using *Punica granatum* peel and its application as a green catalyst for the reduction of an anthropogenic pollutant 4-nitrophenol. *Spectrochim. Acta A* **104**, 262–264. https://doi.org/10.1016/j.saa.2012.11.084.
25. B. Khodadadi, M. Bordbar, and M. Nasrollahzadeh (2017). *Achillea millefolium* L. extract mediated green synthesis of waste peach kernel shell supported silver nanoparticles: application of the nanoparticles for catalytic reduction of a variety of dyes in water. *J. Colloid Interface Sci.* **493**, 85–93. https://doi.org/10.1016/j.jcis.2017.01.012.
26. K. Varunkumar, R. Hussain, G. Hegde, and A. S. Ethiraj (2017). Effect of calcination temperature on Cu doped NiO nanoparticles prepared via wet-chemical method: structural, optical and morphological studies. *Mater. Sci. Semicond. Process.* **66**, 149–156. https://doi.org/10.1016/j.mssp.2017.04.009.
27. M. Bordbar, N. Negahdar, and M. Nasrollahzadeh (2018). *Melissa officinalis* L. leaf extract assisted green synthesis of CuO/ZnO nanocomposite for the reduction of 4-nitrophenol and Rhodamine B. *Sep. Purif. Technol.* **191**, 295–300. https://doi.org/10.1016/j.seppur.2017.09.044.
28. F. Mujeeb, P. Bajpai, and N. Pathak (2014). Phytochemical evaluation, antimicrobial activity, and determination of bioactive components from leaves of *Aegle marmelos*. *Biomed Res. Int.* **2014**, 497606. https://doi.org/10.1155/2014/497606.
29. N. K. R. Bogireddy, K. K. HoskoteAnand, and B. K. Mandal (2015). Gold nanoparticles: synthesis by *Sterculia acuminata* extract and its catalytic efficiency in alleviating different organic dyes. *J. Mol. Liq.* **211**, 868–875. https://doi.org/10.1016/j.molliq.2015.07.027.
30. H. Muthukumar and M. Matheswaran (2015). Amaranthus spinosus leaf extract mediated FeO nanoparticles: physicochemical traits, photocatalytic and antioxidant activity. *ACS Sustain. Chem. Eng.* **3**, 3149–3156. https://doi.org/10.1021/acssuschemeng.5b00722.
31. M. Irfan, M. Moniruzzaman, T. Ahmad, P. Mandal, S. Bhattacharjee, and B. Abdullah (2017). Ionic liquid based extraction of flavonoids from *Elaeis guineensis* leaves and their applications for gold nanoparticles synthesis. *J Mol Liq*. https://doi.org/10.1016/j.molliq.2017.05.151.
32. P. Moteriya and S. Chanda (2017). Synthesis and characterization of silver nanoparticles using *Caesalpinia pulcherrima* flower extract and assessment of their in vitro antimicrobial, antioxidant,

cytotoxic, and genotoxic activities. *Artif. Cells Nanomed. Biotechnol.* **45**, 1556–1567. https://doi.org/10.1080/21691401.2016.1261871.
33. E. Marlina, S. Goh, T. Wu, T. Tan, S. B. AbdHamid, and J. C. Juan (2015). Evaluation on the photocatalytic degradation activity of reactive blue 4 using pure anatase nano-TiO_2. *Sains Malaysiana* **44**, 1011–1019.
34. A. Zielińska-Jurek, M. Klein, and J. Hupka (2017). Enhanced visible light photocatalytic activity of Pt/I-TiO_2 in a slurry system and supported on glass packing. *Sep. Purif. Technol.* **189**, 246–252. https://doi.org/10.1016/j.seppur.2017.08.018.
35. J. H. Lee, J. Hong, J. H. Kim, Y. S. Kang, and S. W. Kang (2012). Facilitated CO_2 transport membranes utilizing positively polarized copper nanoparticles. *Chem. Commun.* **48**, 5298–5300. https://doi.org/10.1039/C2CC17535E.
36. F. Azeez, E. Al-Hetlani, M. Arafa, Y. Abdelmonem, A. Abdel Nazeer, M. Amin, and M. Madkour (2018). The effect of surface charge on photocatalytic degradation of methylene blue dye using chargeable titania nanoparticles. *Sci Rep*. https://doi.org/10.1038/s41598-018-25673-5.
37. N. F. Jaafar, A. A. Jalil, S. Triwahyono, J. Efendi, R. R. Mukti, R. Jusoh, N. W. C. Jusoh, A. H. Karim, N. F. M. Salleh, and V. Suendo (2015). Direct in situ activation of AgO nanoparticles in synthesis of Ag/TiO_2 and its photoactivity. *Appl. Surf. Sci.* **338**, 75–84. https://doi.org/10.1016/j.apsusc.2015.02.106.
38. G. Sujatha, S. Shanthakumar, and F. Chiampo (2020). UV light-irradiated photocatalytic degradation of coffee processing wastewater using TiO_2 as a catalyst. *Environments.* **7**, 47. https://doi.org/10.3390/environments7060047.
39. R. Jiang, H.-Y. Zhu, J.-B. Li, F.-Q. Fu, J. Yao, S.-T. Jiang, and G.-M. Zeng (2016). Fabrication of novel magnetically separable BiOBr/$CoFe_2O_4$ microspheres and its application in the efficient removal of dye from aqueous phase by an environment-friendly and economical approach. *Appl. Surf. Sci.* **364**, 604–612. https://doi.org/10.1016/j.apsusc.2015.12.200.
40. N. Pugazhenthiran, S. Murugesan, P. Sathishkumar, and S. Anandan (2014). Photocatalytic degradation of ceftiofur sodium in the presence of gold nanoparticles loaded TiO_2 under UV–visible light. *Chem. Eng. J.* **241**, 401–409. https://doi.org/10.1016/j.cej.2013.10.069.
41. N. S. Kamarudin, R. Jusoh, A. A. Jalil, H. D. Setiabudi, and N. F. Sukor (2020). Synthesis of silver nanoparticles in green binary solvent for degradation of 2,4-D herbicide: optimization and kinetic studies. *Chem. Eng. Res. Des.* **159**, 300–314. https://doi.org/10.1016/j.cherd.2020.03.025.
42. L. Wang, F. Lu, Y. Liu, Y. Wu, and Z. Wu (2018). Photocatalytic degradation of organic dyes and antimicrobial activity of silver nanoparticles fast synthesized by flavonoids fraction of *Psidium guajava* L. leaves. *J. Mol. Liq.* **263**, 187–192. https://doi.org/10.1016/j.molliq.2018.04.151.
43. M. S. Samuel, S. Jose, E. Selvarajan, T. Mathimani, and A. Pugazhendhi (2020). Biosynthesized silver nanoparticles using *Bacillus amyloliquefaciens*; application for cytotoxicity effect on A549 cell line and photocatalytic degradation of p-nitrophenol. *J. Photochem. Photobiol. B* **202**, 111642. https://doi.org/10.1016/j.jphotobiol.2019.111642.
44. Z. U. H. Khan, N. S. Shah, J. Iqbal, A. U. Khan, M. Imran, S. M. Alshehri, N. Muhammad, M. Sayed, N. Ahmad, A. Kousar, M. Ashfaq, F. Howari, and K. Tahir (2020). Biomedical and photocatalytic applications of biosynthesized silver nanoparticles: ecotoxicology study of brilliant green dye and its mechanistic degradation pathways. *J. Mol. Liq.* **319**, 114114. https://doi.org/10.1016/j.molliq.2020.114114.
45. N. S. Kamarudin, R. Jusoh, N. F. Sukor, A. A. Jalil, and H. D. Setiabudi (2020). Intensified photocatalytic degradation of 2,4-dicholorophenoxyacetic acid using size-controlled silver nanoparticles: effect of pre-synthesis extraction. *Adv. Powder Technol.* **31**, 3381–3394. https://doi.org/10.1016/j.apt.2020.06.023.
46. R. Karthik, M. Govindasamy, S.-M. Chen, Y.-H. Cheng, P. Muthukrishnan, S. Padmavathy, and A. Elangovan (2017). Biosynthesis of silver nanoparticles by using *Camellia japonica* leaf extract for the electrocatalytic reduction of nitrobenzene and photocatalytic degradation of Eosin-Y. *J. Photochem. Photobiol. B* **170**, 164–172. https://doi.org/10.1016/j.jphotobiol.2017.03.018.
47. S. Malini, S. Vignesh Kumar, R. Hariharan, A. Pon Bharathi, P. Renuka Devi, and E. Hemananthan (2020). Antibacterial, photocatalytic and biosorption activity of chitosan nanocapsules embedded with *Prosopis juliflora* leaf extract synthesized silver nanoparticles. *Mater. Today Proc.* **21**, 828–832. https://doi.org/10.1016/j.matpr.2019.07.587.
48. J. Singh, V. Kumar, S. Singh Jolly, K.-H. Kim, M. Rawat, D. Kukkar, and Y. F. Tsang (2019). Biogenic synthesis of silver nanoparticles and its photocatalytic applications for removal of organic pollutants in water. *J. Ind. Eng. Chem.* **80**, 247–257. https://doi.org/10.1016/j.jiec.2019.08.002.
49. B. Kumar, K. S. Vizuete, V. Sharma, A. Debut, and L. Cumbal (2019). Ecofriendly synthesis of monodispersed silver nanoparticles using Andean Mortiño berry as reductant and its photocatalytic activity. *Vacuum.* **160**, 272–278. https://doi.org/10.1016/j.vacuum.2018.11.027.
50. J. Mangalam, M. Kumar, M. Sharma, and M. Joshi (2019). High adsorptivity and visible light assisted photocatalytic activity of silver/reduced graphene oxide (Ag/rGO) nanocomposite for wastewater treatment. *Nano-Struct. Nano-Objects.* **17**, 58–66. https://doi.org/10.1016/j.nanoso.2018.11.003.
51. S. Shukla, S. Chaudhary, A. Umar, G. R. Chaudhary, S. K. Kansal, and S. K. Mehta (2016). Surfactant functionalized tungsten oxide nanoparticles with enhanced photocatalytic activity. *Chem. Eng. J.* **288**, 423–431. https://doi.org/10.1016/j.cej.2015.12.039.
52. S. Talebi, N. Chaibakhsh, and Z. Moradi-Shoeili (2017). Application of nanoscale ZnS/TiO_2 composite for optimized photocatalytic decolorization of a textile dye. *J. Appl. Res. Technol.* **15**, 378–385. https://doi.org/10.1016/j.jart.2017.03.007.
53. R. Begum, K. Naseem, E. Ahmed, A. Sharif, and Z. H. Farooqi (2016). Simultaneous catalytic reduction of nitroarenes using silver nanoparticles fabricated in poly(N-isopropylacrylamide-acrylic acid-acrylamide) microgels. *Colloids Surf. A* **511**, 17–26. https://doi.org/10.1016/j.colsurfa.2016.09.076.
54. R. Begum, J. Najeeb, G. Ahmad, W. Wu, A. Irfan, A. G. Alsehemi, and Z. H. Farooqi (2018). Synthesis and characterization of poly(N-isopropylmethacrylamide-co-acrylic acid) microgels for in situ fabrication and stabilization of silver nanoparticles for catalytic reduction of o-nitroaniline in aqueous medium. *React. Funct. Polym.* **132**, 89–97. https://doi.org/10.1016/j.reactfunctpolym.2018.09.004.
55. M. Shirzad-Siboni, A. Jonidi-Jafari, M. Farzadkia, A. Esrafili, and M. Gholami (2017). Enhancement of photocatalytic activity of Cu-doped ZnO nanorods for the degradation of an insecticide: kinetics and reaction pathways. *J. Environ. Manage.* **186**, 1–11. https://doi.org/10.1016/j.jenvman.2016.10.049.
56. G. M. S. ElShafei, A. M. Al-Sabagh, F. Z. Yehia, C. A. Philip, N. A. Moussa, G. Eshaq, and A. E. ElMetwally (2018). Metal oxychlorides as robust heterogeneous Fenton catalysts for the sonophotocatalytic degradation of 2-nitrophenol. *Appl. Catal. B* **224**, 681–691. https://doi.org/10.1016/j.apcatb.2017.11.015.

Publisher's Note Springer Nature remains neutral with regard to jurisdictional claims in published maps and institutional affiliations.